ISPRS Journal of Photogrammetry and Remote Sensing 93 (2014) 40–48

Contents lists available at ScienceDirect

ISPRS Journal of Photogrammetry and Remote Sensing

journal homepage: www.elsevier.com/locate/isprsjprs

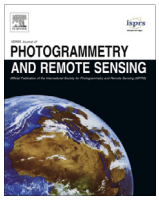

# A review of ground-based SAR interferometry for deformation measurement

O. Monserrat *, M. Crosetto, G. Luzi

*Centre Tecnològic de Telecomunicacions de Calalunya (CTTC), Division of Geomatics, Castelldefels, Spain*

ARTICLE INFO

*Article history:*
Received 19 September 2013
Received in revised form 31 March 2014
Accepted 1 April 2014
Available online 4 May 2014

*Keywords:*
SAR
Interferometry
Terrestrial
Deformation
Monitoring
Review

ABSTRACT

This paper provides a review of ground-based SAR (GBSAR) interferometry for deformation measurement. In the first part of the paper the fundamentals of this technique are provided. Then the main data processing and analysis stages needed to estimate deformations starting from the GBSAR observations are described. This section introduces the two types of GBSAR acquisition modes, i.e., continuous and discontinuous GBSAR, and reviews the different GBSAR processing and analysis methods published in the literature. This is followed by a discussion of the specific technical aspects of GBSAR deformation measurement. A section then summarizes the pros and cons of GBSAR for deformation monitoring. The last part of the paper includes two reviews: one concerning the GBSAR systems described in the literature, including non-strictly SAR systems and a second one addresses the main GBSAR applications.



## 1. Introduction

This paper provides a review of ground-based SAR (GBSAR) interferometry for deformation measurement. In the last decade this technique has gained an increasing interest as a deformation measurement and monitoring tool. This is due to its specific characteristics, which make it complementary to many other existing deformation monitoring techniques.

The GBSAR is a radar-based terrestrial remote sensing imaging system (Tarchi et al., 1999). It consists of a radar sensor that emits and receives a burst of microwaves, repeating this operation while the sensor is moving along a rail track (Noferini, 2004; Bernardini et al., 2007). The imaging capability is achieved by exploiting the Synthetic Aperture Radar (SAR) technique, e.g., see Hanssen (2001). The length of the rail determines the cross-range resolution of the acquired images: the longer the rail, the higher the cross-range resolution. The GBSAR is based on a coherent radar system, which measures not only the amplitude but also the phase of the received radar signal. The phase measurements can be exploited, by using interferometric techniques, to derive information on the deformation and topography of the measured scene. The main GBSAR application is deformation monitoring. Its high sensitivity to small deformations, the long range of its measurements (up to several kilometres) and its imaging capability, which allows the system to perform simultaneously a vast number of measurements, are interesting characteristics that make the GBSAR system complementary to other deformation measurement techniques.

This paper is focused on the interferometric use of GBSAR. However, it is worth mentioning that a non-interferometric GBSAR approach to derive deformation estimates has been recently published (Crosetto et al., 2014; Monserrat et al., 2013). This approach exploits the geometric content of GBSAR amplitude imagery and estimates deformation through image matching. It is less sensitive to deformation but it offers the advantages of yielding aliasing-free deformation estimates, which, in addition, are insensitive to atmospheric effects.

This paper is organized as follows. Section 2 recalls the fundamentals of GBSAR interferometry for deformation measurement. Section 3 discusses the main GBSAR data processing and analysis aspects and the technical issues related to GBSAR deformation measurement. Section 4 discusses the pros and cons of GBSAR for deformation measurement and monitoring. Section 5 reviews the GBSAR systems described in the literature including also non-strictly SAR systems. Section 6 treats the main GBSAR deformation measurement applications. Conclusions follow.

## 2. GBSAR interferometry

This section recalls the working principle and some related aspects of GBSAR interferometry for deformation measurement.

* Corresponding author. Address: Oriol Monserrat, Centre Tecnològic de Comunicacions de Catalunya-Geomatics Division, Parc Mediterrani de la Tecnologia, Av. Gauss 11, E-08860 Castelldefels, Barcelona, Spain. Tel.: +34 935569291; fax: +34 935569292.

*E-mail address:* oriol.monserrat@cttc.es (O. Monserrat).

http://dx.doi.org/10.1016/j.isprsjprs.2014.04.001

The GBSAR is an imaging sensor. In this paper the SAR techniques used to provide the complex radar image are not discussed and readers are relegated to literature, see for instance: Fortuny and Sieber (1994), Tarchi et al. (2003a), Fortuny-Guasch (2009) and Reale et al. (2009). For each image pixel a GBSAR provides a complex number, which consists of the In-phase and Quadrature (I and Q) components of the received echo, from which the signal phase $\varphi$ and amplitude $A$ can be derived.

The amplitude is mainly used to interpret the image scene and to study the backscattering characteristics of the monitored area, e.g., see Ulaby et al. (1986). The phase can be exploited for deformation measurement, which is the subject of this paper, or for digital elevation model generation (Pieraccini et al., 2001; Nico et al., 2004; Nico et al., 2005; Noferini et al., 2007; Rödelsperger et al., 2010). Note that, with respect to spaceborne interferometry, in ground based observations the deformation measurement is usually performed using a zero-baseline configuration, i.e., all images are taken from the same position. By contrast, when GBSAR measurements are aimed at DEM generation, a non-zero baseline configuration is needed (Noferini et al., 2007). Let's consider a deformation measurement scenario, observed twice by a GBSAR system. Let's take the phases $\varphi_1$ and $\varphi_2$ of two homologous pixels (i.e., pixels that correspond to the same target) from two images acquired at different times:

$$\begin{aligned}\varphi_1 &= \varphi_{geom-1} + \varphi_{scatt-1} = \tfrac{4\cdot\pi\cdot R_1}{\lambda} + \varphi_{scatt-1}\\ \varphi_2 &= \varphi_{geom-2} + \varphi_{scatt-2} = \tfrac{4\cdot\pi\cdot R_2}{\lambda} + \varphi_{scatt-2}\end{aligned} \quad (1)$$

where $R_1$ and $R_2$ are the sensor to target distances at each acquisition, $\varphi_{scatt}$ is the phase shift generated during the interaction between the microwaves and the target, $\lambda$ the wavelength of the emitted signal, and the factor $4\pi$ is related to the two way path, radar-target-radar. Neglecting the signal propagation effects, the interferometric phase $\Delta\varphi_{21}$, which is the main GBSAR observation, is given by:

$$\Delta\varphi_{21} = \varphi_2 - \varphi_1 = \frac{4\cdot\pi\cdot(R_2 - R_1)}{\lambda} + (\varphi_{scatt-2} - \varphi_{scatt-1}) \quad (2)$$

If the phase shift components $\varphi_{scatt\text{-}2}$ and $\varphi_{scatt\text{-}1}$ remain constant between the two acquisitions (i.e., its variation over time is negligible), $\Delta\varphi_{21}$ is directly related to the distance difference ($R_2$-$R_1$) and hence to the target displacement. In practice, there are at least four other terms:

$$\begin{aligned}\Delta\varphi_{21} &= \varphi_2 - \varphi_1\\ &= \varphi_{defo} + (\varphi_{atmo2} - \varphi_{atmo1}) + \varphi_{geom} + \varphi_{noise} + 2\cdot k\cdot\pi\end{aligned} \quad (3)$$

where $\varphi_{defo}$ is the component related to the displacement, ($\varphi_{atmo2}-\varphi_{atmo1}$) is the phase component due to the atmospheric effects during image acquisition; $\varphi_{geom}$ contains the geometric phase component due to repositioning errors between the two image acquisitions; $\varphi_{noise}$ is the phase component related to the term ($\varphi_{scatt\text{-}2}-\varphi_{scatt\text{-}1}$) and other noise sources, like instrumental noise; finally the term $2\cdot k\cdot\pi$ is due to the fact that $\Delta\varphi_{21}$ is wrapped, i.e., bounded in the range $[-\pi, \pi]$, where $k$ is an integer value. Eq. (3) is the main observation equation of GBSAR for deformation measurement. It is similar to the equation used for satellite SAR interferometry observations, e.g., see Crosetto et al. (2005), where the $\varphi_{geom}$ term corresponds to the orbital phase component. In addition, as already mentioned above, Eq. (3) does not contain the topographic phase component because GBSAR acquisitions are usually performed using a zero-baseline configuration.

## 3. GBSAR data processing and analysis

Deriving deformation estimates from the GBSAR interferometric phases is often not a trivial task. In the following section we describe the main data processing and analysis stages needed to estimate deformations. This is followed by a section that describes the specific technical aspects of GBSAR deformation measurement, which are essential to properly understand the pros and cons of this technique.

Before considering the main GBSAR processing stages, it is worth mentioning that GBSAR data can be acquired using two types of acquisition modes: the continuous (C-GBSAR) and the discontinuous (D-GBSAR). In the former one, which represents the most commonly used configuration, the instrument is left installed in situ, acquiring data on a regular base, e.g., every a few minutes. In the latter one the instrument is installed at each campaign, revisiting a given site periodically, e.g., weekly, monthly or yearly, depending on the kinematics of the deformation event at hand, e.g., see Noferini et al. (2008) and Luzi et al. (2010a). C-GBSAR allows the user to have a "near real-time" monitoring of the site of interest, e.g., see Tarchi et al. (2005): it is appropriate to measure fast deformation phenomena, e.g., with displacements ranging from some mm/day to m/day, providing a monitoring tool that can support the management of emergency scenarios, e.g., see Casagli et al. (2003), Tarchi et al. (2003a) and Tarchi et al. (2005). By contrast, D-GBSAR can be adequate to monitor slow deformation phenomena, where C-GBSAR cannot be used due to either logistic or cost reasons. As it is discussed later in this paper, there are substantial technical differences between C-GBSAR and D-GBSAR.

### 3.1. Main GBSAR processing stages

This section describes the main processing and analysis stages needed to derive GBSAR deformation measurements. Even though there are differences between the processing chains used by different authors, they use most of the stages described below.

#### 3.1.1. Image co-registration

GBSAR interferometry requires properly co-registered SAR images, i.e., pixels with equivalent location in the images have to match the same footprint on the ground. This stage can usually be highly automated, unless there are significant changes between the analysed images. Different algorithms can be found in the literature, e.g., see Lin et al. (1992) and Hanssen (2001). Co-registration is mandatory with D-GBSAR, especially if "light positioning" is performed, e.g., by simply materializing the GBSAR location using some marks. Note that this is necessary in many practical cases, e.g., where a concrete base or any other precise mechanical positioning structure cannot be employed. In principle, the co-registration can be avoided using C-GBSAR. However, measuring at long distances and with long data acquisition times, the co-registration can be useful to compensate, at least partially, the image distortions due to atmospheric variations occurring during the acquisition of single images (Martínez-Vazquez, 2008).

#### 3.1.2. Interferogram and coherence image generation

From the stack of N co-registered GBSAR images, the interferograms and the associated coherence images are generated. This is preceded by the design of the interferogram network, which defines how the $N$ images are connected through a set of $M$ interferograms. Often zero-redundancy networks are used, e.g., $N-1$ interferograms that connect consecutive images, e.g., see Noferini et al. (2005a). More complex and redundant networks can be used to reduce error propagation due to 2D-phase unwrapping errors (Crosetto et al., 2011).

#### 3.1.3. Pixel selection

The goal of pixel selection is identifying the pixels characterized by low $\varphi_{Noise}$, where the interferometric phase can be exploited. The most used selection criteria are the coherence-based, e.g., see Berardino et al. (2002), and the amplitude-based selection (Ferretti et al., 2001). Both criteria make use of an appropriate threshold, which is usually fixed by adjusting the trade-off between phase quality and density of the selected pixels. An empirical way to check the goodness of this threshold is to assess the results of phase unwrapping (Monserrat, 2012).

#### 3.1.4. 2D phase unwrapping

In this step the wrapped interferometric phases of the generated interferograms are unwrapped. This operation is usually performed interferogram by interferogram, without exploiting the time component and involving a 2D phase unwrapping, e.g., see Ghiglia and Pritt (1998). An alternative approach is to make 1D phase unwrapping over time, which is made after performing phase integration (Noferini et al., 2005a; IDS, 2013).

#### 3.1.5. Phase integration

In this step, starting from the set of interferograms, the phases in correspondence to each acquired image are estimated. They are the accumulated phases with respect to the first image which contains three main components: deformation, $\varphi_{atmo}$ and $\varphi_{geom}$. The direct integration is the simplest way to reconstruct the N phases, which requires the minimum set of interferograms to connect all the images (Noferini et al., 2005a; IDS, 2013). As mentioned above, more advanced strategies can be implemented to detect and correct for 2D phase unwrapping errors during phase integration (Crosetto et al., 2011).

#### 3.1.6. Estimation of the atmospheric phase component

In this stage $\varphi_{atmo}$ and $\varphi_{geom}$ are estimated and separated from the deformation component. Note that these two phase components are usually estimated together as they have similar statistical characteristics: both vary smoothly in space. Different approaches have been proposed in the literature. Luzi et al. (2004) and Noferini et al. (2005a) assume $\varphi_{atmo}$ to be a function of range and use one or two points of the scene, which are known to be stable, to estimate a linear or quadratic term, respectively. Rödelsperger (2011) and Iannini and Guarnieri (2011) estimate $\varphi_{atmo}$ using meteorological observations (temperature, humidity and pressure). Luzi et al. (2010a) make use of 2D-polynomials, whose coefficients are estimated by least squares adjustment using stable areas of the measured scene, which have to be known a priori. It is worth noting that the estimation of $\varphi_{atmo}$ is not always trivial, especially in areas that are topographically non-homogeneous (Monserrat, 2012). For areas with steep topography Iglesias et al. (2013) propose a 2D multiple regression model (height-dependent).

#### 3.1.7. Displacement computation and geocoding

This stage is fundamental for GBSAR data interpretation and exploitation, e.g., see Leva et al. (2005) and Noferini et al. (2008). Firstly, the interferometric phases, which refer to the line between the sensor and the measured object, the radar Line-of-Sight (LOS), are transformed into LOS displacements. Then, the geocoding is performed, which involves a transformation from the image space, where each pixel is identified by its position in the image, to the object space, by assigning cartographic coordinates ($E$, $N$) or geographic coordinates ($\varphi$, $\lambda$), plus an orthometric or ellipsoidal height, or simply a local Cartesian system, $X$, $Y$, $Z$ (Rödelsperger et al., 2010).

### 3.2. Discussion of main technical issues

This section discusses some technical issues related to GBSAR deformation measurement. They are fundamental to properly understand and exploit this technique.

#### 3.2.1. The role of phase noise

Even though GBSAR delivers raster products, only those pixels that are characterized by small noise contribution $\varphi_{Noise}$ can be exploited to estimate deformations. $\varphi_{Noise}$ depends on the physical and geometric characteristics of the measured objects and their changes between the GBSAR image acquisitions. The interferometric phase quality is usually measured by the so-called coherence: the lower $\varphi_{Noise}$, the higher the coherence. Significant improvements of the coherence can be obtained by using polarimetric GBSAR data (Iglesias et al., 2013; Pipia et al., 2013). Obtaining a sufficiently high coherence is a critical problem for D-GBSAR. Fig. 1 illustrates an example related to a landslide: Fig. 1b shows the coherent points (coherence above 0.9) from C-GBSAR with time lapse between the two images of several hours, while Fig. 1c shows D-GBSAR data over the same area, with time lapse of one month. In the latter case, only the manmade rock wall remains coherent: this shows how severe the coherence loss can be for D-GBSAR. This limitation is similar to the one of satellite-based repeat-pass SAR interferometry, e.g., see Hanssen (2001). The deformation monitoring of low coherent areas can be achieved using artificial Corner Reflectors (CRs), which guarantee observations characterized by low $\varphi_{Noise}$, e.g., see Luzi et al. (2010a).

#### 3.2.2. Phase unwrapping

The correct deformation estimation implies the reconstruction of the full phase value, by estimating the integer number of cycles $k$ to be added to the wrapped phase. This operation, named phase unwrapping, has infinite solutions (Ghiglia and Pritt, 1998): this represents an intrinsic limitation from the deformation measurement viewpoint. Most of the phase unwrapping algorithms assume that the full interferometric phases (i.e., the unwrapped phases) vary smoothly over a given interferogram and satisfy this condition:

$$|\Delta\varphi_{12\_unwr}(i,j) - \Delta\varphi_{12\_unwr}(k,l)| < \pi \tag{4}$$

where $(i, j)$ and $(k, l)$ represent two neighbouring coherent pixels. If this requirement is not satisfied, phase unwrapping errors that are multiple of $2\pi$ can occur and, as a consequence, severe errors can affect the deformation estimates. Considering that $2\pi$ corresponds to a displacement of half wavelength, the above condition can be expressed in terms of displacements:

$$|Defo\_\Delta t(i,j) - Defo\_\Delta t(k,l)| < \frac{\lambda}{4} \tag{5}$$

where is the wavelength corresponding to the centre operating frequency of the radar, and $Defo\_\Delta t$ is the deformation occurring between two image acquisitions. This condition is particularly critical for D-GBSAR applications: it requires to properly adjust the observation time interval $\Delta t$. It is worth noting that Eqs. (4) and (5) refer to phase or deformation differences, and not to absolute values. Note that the same equations hold for satellite-based SAR interferometry applications, e.g., see Crosetto et al. (2011).

#### 3.2.3. 1D deformation measurements

The GBSAR deformation measurements refer to the LOS. This represents an important limitation of the technique with respect to other techniques able to estimate the full 3D deformation field. It is worth mentioning that the amplitude-based approach proposed by Crosetto et al. (2014) is in principle able to provide 2D deformation estimates (in range and cross-range directions). Considering the LOS, particular attention is needed in choosing

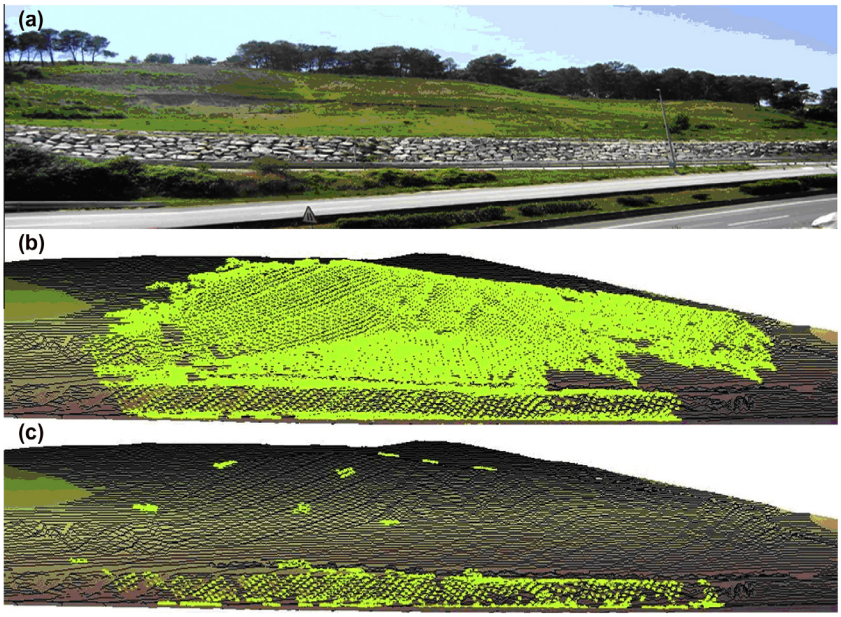


**Fig. 1.** Role of coherence in C-GBSAR and D-GBSAR acquisition modes. Photograph of a landslide (a). Geocoded coherent points (in green) from C-GBSAR, with time lapse between acquisitions of several hours (b). Geocoded coherent points (in green) from D-GBSAR, with 1-month time lapse (c).

the location of the GBSAR: the ideal case is to have the LOS direction parallel to the displacement direction, while the worst case occurs when they are almost perpendicular. For instance, this occurs in a flat area when a subsidence area is observed by a GBSAR located at the same height.

*3.2.4. Relative deformation measurements*

GBSAR deformation measurements are relative to a given reference point located in the imaged scene. The need of a reference point could in principle be avoided under this ideal condition: the atmosphere between the GBSAR and the scene is perfectly stable over time or its physical properties (humidity, temperature and pressure) are accurately monitored during image acquisitions so that the term $\varphi_{atmo}$ in Eq. (3) can be accurately estimated for each interferogram pixel. This can hardly be accomplished in practice. For this reason we usually need to identify a reference point in the measured scene and refer all the deformations to it. This is usually done by choosing a point in a stable area; if this is unavailable, any arbitrary pixel in the scene can be chosen bearing in mind that all other measurements refer to this point.

## 4. Pros and cons of GBSAR for deformation monitoring

This section discusses the main pros and cons of the GBSAR technique for deformation measurement. The main advantages of GBSAR are briefly discussed below.

- The GBSAR technique offers a flexible and versatile tool suitable to monitor deformation phenomena characterized by a wide range of deformation rates, which roughly ranges from a few millimetres per year up to one metre per hour (Leva et al. 2003).
- The precision of the GBSAR deformation estimates ranges from sub-millimetres to a few millimetres: this depends on the characteristics of the target (the stronger its response, the better is the precision), the sensor to target distance, and the distance from the reference point. A precision below 1 mm, which was estimated on artificial targets, is described in Takahashi et al. (2013).
- The technique has the capability of independently measuring the atmospheric conditions at distances up to some kilometres. This is a key advantage with respect to other sensors like terrestrial laser scanners or topographic total stations, which are strongly affected by meteorological phenomena like fog, wind and rain.
- A GBSAR image can typically cover an area of 1–2 km$^2$, providing, over coherent areas, a dense measurement coverage of the observed scene (Leva et al. 2003; Tarchi et al., 2005). The dense sampling capability represents an advantage with respect to point-like measurement techniques, like GPS, total stations, etc. (Casagli et al., 2003).
- The whole GBSAR deformation monitoring process can be highly automated. It can be used as an operational monitoring tool, even during emergencies (Casagli et al., 2003; Tarchi et al., 2003a). It is worth noting that the instrumentation can be installed outside the target area: this is an advantage especially when dangerous deformation phenomena have to be monitored.

Some of the main limitations of GBSAR are listed below.

- GBSAR interferometry requires, as necessary condition, coherent data. This is a critical issue in several application scenarios, especially for D-GBSAR. For this reason, it is recommended to carry out a feasibility study before planning any new D-GBSAR survey. In some cases the lack of coherence can be overcome by deploying artificial CRs, e.g., see Luzi et al. (2010a) or Iglesias et al. (2013).
- A critical limitation of the technique is related to the ambiguous nature of the interferometric phases, which can cause biased deformation estimates, especially in those areas that suffer the largest displacements (Crosetto et al., 2014). This limitation is especially problematic for D-GBSAR measurements. A non-interferometric GBSAR approach has been recently proposed, which is less sensitive to deformation but yields aliasing-free deformation estimates (Crosetto et al., 2014; Monserrat et al., 2013).

**Table 1**
Available systems based on the radar technique that are described in literature. Characteristics have been taken from published papers cited in the table. In the lower part of the table non-strictly SAR systems are listed.

| Owner/customer | Name | Goal | Radar type | Band | Pol. | Acquisition time for one image | Scan geometry | Range resolution (m) | Azimuth resolution[4] (mrad) or (m) @ 1 km | Nominal precision (mm) |
|---|---|---|---|---|---|---|---|---|---|---|
| JRC (EC)[1] | Lisa | Research | VNA based | C<br>Ku | VV, HH<br>VH, HV | 30 min | Linear | 0.5 | 3 | 0.02–4 |
| Ellegi srl, formerly Lisalab (I)[5] | Lisa | Market | VNA based | Ku | VV | 12 min | Linear | 0.5 | 3 | 0.01–3.2 |
| UNIFI DET (I)[3] | – | Research | VNA based | S, C | VV | 25 min | Linear | 0.5 | 20-dic | 2 |
| Technical University of Catalonia (UPC)[8] | RiskSAR | Research | FMCW | X | VV, HH | 1 min (single pol) | Linear | 1.25 | 4 | 1.6 |
| | – | | | | VH, HV | | | | | |
| IDS spa (I)[7] | IBIS-L/M | Market | SFCW | Ku | VV | 8 min | Linear | 0.5/0.75 | 4.4 | 0.03–4 |
| Tohoku University (J)[4] | – | Research | VNA based | S, C<br>X | VV, HH<br>VH, HV | 2 min | Linear | 0.4 | 5 | 2. |
| Centre for Earth Obs. Sci., Sheffield Univ./Cranfield Univ. (UK)[2] | – | Research | VNA based | C, X | VV, HH | NA | Linear | NA | NA | NA |
| | | | | | VH, HV | | | | | |
| KIGAM Korean Institute of Geoscience and Mineral Resources (KOR)[6] | – | Research | VNA based | C | VV, HH | NA | Arc | 0.25 | 2 | 0.4 |
| | | | | | VH, HV | | | | | |
| Institute for radiophysics and electronics (UA)[10] | GB NW-SAR | Research | Noise radar | Ka | VV | 20 s | Angular | 1 | 12 | NA |
| MetaSensing (NL)[9] | FastGBSAR | Research/ market | FMCW | Ku | NA | 5 s | Linear | 0.5 | 4.5 | 0.1 |
| *Nonstrictly SAR GB systems* | | | | | | | | | | |
| GAMMA remote sensing AG (CH)[12] | GPRI | Research/ market | FMCW mechanical scanning | Ku | VV | 30 min (90° scan) | Angular | 0.75 | 7 | 0.02–4 |
| JRC (EC)[11] | Melissa | Research | MIMO | Ku | VV | 0.36 s | No motion | | | |
| GROUNDPROBE (AUS)[13] | SSR | Market | Mechanical Scanning | Ku | VV | 15 min | Angular Non-SAR | 0.75 | 9 | 0.03–3.5 |

- The applicability of the technique is limited by the LOS nature of the GBSAR sensor: displacements perpendicular to the LOS cannot be measured. In some scenarios, e.g., monitoring vertical displacements in a completely flat area, this constraint can strongly limit the usability of the technique. In addition, the 1D LOS nature of deformation measurements represents a limitation with respect to other techniques that can provide 3D deformation measurements, like total stations, GPS, etc.
- The correct estimation of $\varphi_{atmo}$ requires the availability of stable areas in the surroundings of the deformation area of interest (Monserrat, 2012). In some scenarios this requirement cannot be fulfilled, e.g., this occurs when there is a cluster of coherent pixels, which is isolated from the other coherent areas. In such cases, it is often impossible to properly estimate $\varphi_{atmo}$, and this hampers considerably the deformation measurement capability of the technique.

## 5. GBSAR system review

This section makes a short review of the GBSAR systems described in the literature. A GBSAR is a microwave electronic system basically composed of a radar sensor, an acquisition technique and the related data processing, namely the focusing algorithms (Luzi et al., 2010b). The core of the radar sensor, in the pioneer GBSAR systems, was a Vectorial Network Analyzer (VNA) (Leva et al., 2003[1][1]; Brown et al., 2003[2]; Luzi et al., 2004[3]; Zhou et al., 2004[4]; Del Ventisette et al., 2011[5]; Lee et al., 2013[6]), a laboratory instrument purchasable from microwave instrumentation companies, which is equivalent to powerful and versatile coherent radar that is operating as Step Frequency Continuous Wave (SFCW) radar. In the last ten years this option has been replaced by specifically developed prototypes (Bernardini et al., 2007)[7], using Frequency Modulation Continuous Radars (FMCW), see Iglesias et al. (2013)[8], made directly by the companies and the research teams developing their own GBSAR. This upgrade not only improves the manageability of the instrument, but also reduces the acquisition times, down to less than a minute (Meta and Trampuz, 2009)[9], and costs as well. The recent development of very fast sensors based on FMCW radar, Noise radar (Lukin et al., 2009[10]; Tarchi et al., 2010) and MIMO technology (Tarchi et al., 2013)[11], drastically reduce the coherence problem during image acquisitions. Nevertheless, due to the high flexibility of the VNA based system, this kind of approach still persists in many research systems. A short explanation of the basic relationships between system characteristics and performances of the provided SAR image, as spatial resolutions, operating range, etc., can be found for example in Tarchi et al. (2003b) and Luzi et al. (2004)[3]. SAR systems achieve the synthetic aperture through the motion of the radar sensor. The linear scanning obtained moving the sensor along a rail is the solution adopted for the majority of the systems, except for some recent systems where angular scanning is used, e.g., see Lee et al. (2013)[6] and Lukin et al. (2009)[10]. Strictly linked to the radar type and the scanning mode is the applied focusing algorithm. The focusing algorithm must transform the acquired raw data, consisting of a matrix of complex numbers, into a radar image; satellite and GBSAR are based on the same physical principle but their respective acquisition geometries and temporal characteristics require some differences in the focusing algorithms and the available performances. For this reason, in the GBSAR case, the azimuth resolution is non-optimal and depends on the target to sensor distance. A discussion about this topic is out of the scope of this paper, we only observe that since the first algorithms

[1] The numbers in the square bracket used in this section refer to the references in Table 1.

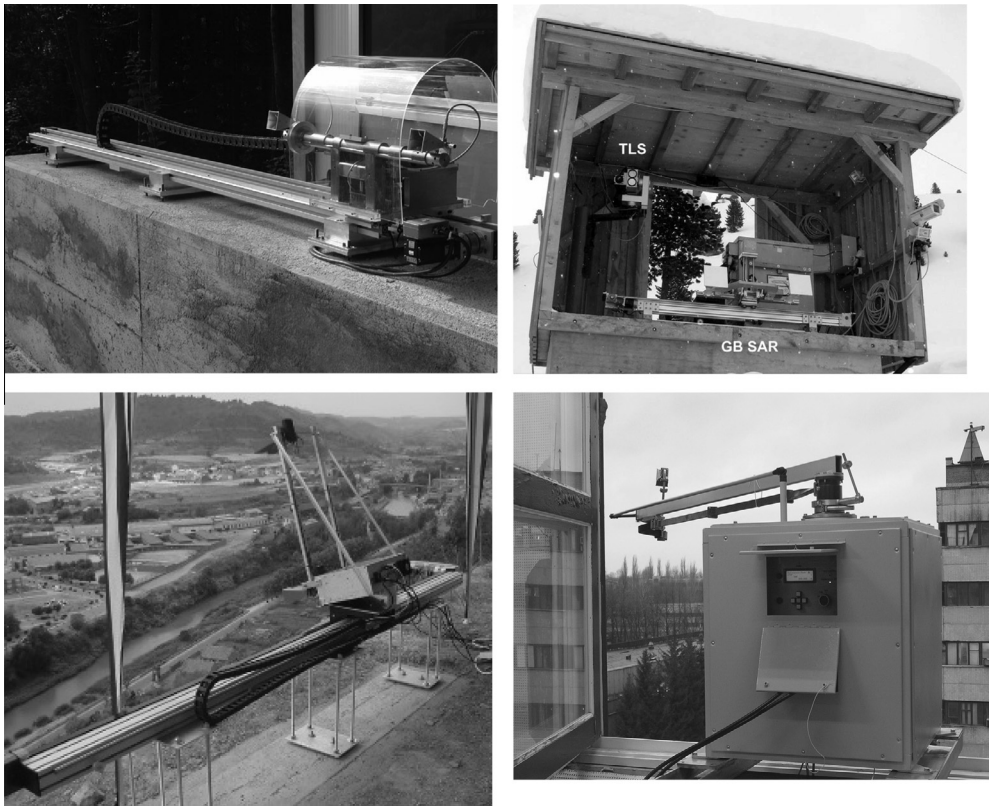


**Fig. 2.** Photographs of four GBSAR prototypes cited in Table 1, developed by research institutions. Prototype of Lisa developed by JRC-EC [1], upper left; GBSAR developed at the University of Florence (Italy) [3], upper right; the RiskSAR system developed by the Technical University of Catalonia (UPC), Barcelona (Spain) [8], lower left; and the GBSAR with angular scanning, developed by the Institute for Radiophysics and Electronics, Kharkov (Ukraine) [10] lower right.

specifically addressed GBSAR systems, e.g., Fortuny and Sieber (1994), several algorithms have been developed; a summary can be found in Ozdemir et al. (2011). Several aspects of the GBSAR system are addressed by the MIT Lincoln laboratory web page (http://www.ll.mit.edu/news/iapradarcourse.html), where interesting educational material can be downloaded.

Table 1 resumes, to the authors' knowledge, the main GBSAR systems described in literature. The characteristics have been taken from published papers cited in the table. In the lower part of the table non-strictly SAR systems are listed (Strozzi et al., 2012[12]; Noon and Harries, 2007[13]), which however can provide complex radar images, which can be processed for deformation monitoring through interferometry. A comparison between the SAR and mechanical scanning performances is briefly discussed in Pieraccini (2013). To conclude, in Fig. 2 are shown four of the systems described in Table 1.

## 6. Review of deformation measurement applications

In this section, we briefly review the main GBSAR applications. Since the first paper on GB-SAR for structure monitoring (Tarchi et al., 1999[14]),[2] many deformation measurement applications of this technique have been developed.

Table 2 shows a classification of the GBSAR applications grouped by the type of application and type of monitoring: C-GBSAR or D-GBSAR. The most consolidated application is the C-GBSAR slope monitoring in open pit mines. Although it could be included in the wider application field of landslide monitoring, it deserves to be mentioned apart. In fact, in the open pit mine field, the GBSAR technique has experienced a strong development at both system and data processing levels providing an operational early warning tool, e.g. see (Farina et al., 2011[15]; Farina et al., 2012[16]; Mecatti et al. 2010[17]; and Severin et al., 2011[18]; Noon and Harries, 2007). The capability of measuring several thousands of points every few minutes and detecting small and local changes is fundamental in this application (Farina et al., 2013[19]; Mecatti et al., 2010[17]).

The monitoring of slope instability related to different phenomena, like rockslides (Tarchi et al., 2005[20]), landslides (Tarchi et al., 2003b[21]; Luzi et al., 2006; Herrera et al., 2009[22]; Corsini et al., 2013[23]; Barla et al., 2010[24]; Schulz et al., 2012[25]) or volcanoes (Casagli et al. 2010[26]; Luzi et al., 2010b; Bozzano et al., 2011[37]; Intrieri et al., 2013[27]) is another major GBSAR application. Although this application is one of the most described in the literature and it has been successfully applied over different sites, it still requires improvements related to technical and logistical aspects. From the technical point of view, most of the systems available nowadays work with Ku-band: this allows high resolution and high displacement sensitivity to be obtained with acceptable hardware performances (Leva et al. 2003[28]; Rödelsperger, 2011[29]). However, the Ku-band is very sensitive to small changes in the observed scene, which are common in natural environments and which can cause coherence loss (Leva et al., 2003[28]; Luzi et al., 2004[3]). Furthermore, the loss of coherence can increase the risk of aliasing (Luzi et al., 2010a[30]; Monserrat, 2012[31]). Coherence loss affects particularly D-GBSAR (Noferini et al., 2005b[13]; Luzi et al., 2010a[30]); however it can also appear for C-GBSAR. A possible improvement could be obtained by using lower frequencies, at the price of loosing precision and resolution, e.g., see (Herrera et al., 2009[22]; Iglesias et al., 2013[8]). Another important issue to be improved in landslide and slope monitoring, especially using D-GBSAR, is atmospheric modelling. Although several authors have proposed different approaches (Noferini et al., 2008[32]; Iglesias et al., 2013[8]; Iannini and Guarnieri, 2011[33]; Rödelsperger,

[2] The numbers in the square bracket used in this section refer to the references in Table 2.

**Table 2**
Classification of the main GBSAR applications grouped by the type of application and type of monitoring: C-GBSAR or D-GBSAR.

| | C-GBSAR | | | D-GBSAR | | |
|---|---|---|---|---|---|---|
| | State of the art | Pros | Cons and aspects to be improved | State of the art | Pros | Cons and aspects to be improved |
| Open pit slope stability monitoring | Consolidated and operational [15,16,17] | Early warning system, [19] spatial and temporal sampling, weather independent, synoptic view [18] | Unhomogeneus atmosphere effects, loss of coherence | Research | Spatial sampling, weather independent | Loss of coherence, risk of aliasing, unhomogeneus atmosphere effects |
| Landslides | Consolidated [20,26,37,24] and operational [27] | Spatial and temporal sampling [20], long range [26], early warning system [21], weather independent [26] | Loss of coherence [1,30], unhomogeneus atmosphere effects [29,33], phase unwrapping | Research [8,30, 32, 23] | Long range measurements [30,32], spatial sampling [30,32] | Loss of coherence [30,32], risk of aliasing [30,32], unhomogeneus atmosphere effects [8] |
| Urban monitoring and single building | Consolidated [34,35,45] | Spatial and temporal sampling, high sensitivity to small displacements [35], non-invasive [34] | Acquisition geometry, precise geocoding [35, 41], other disturbance signals (e.g., thermal dilations [31]), cost | Research [36] | Spatial and temporal sampling, high sensitivity to small displacements, non-invasive [30,36] | Acquisition geometry, precise geocoding [35, 41], other disturbance signals (e.g., thermal dilations), costs |
| Structure monitoring | Consolidated [31,38–40] | Temporal sampling, high sensitivity to small displacements [29,31,40], non-invasive [29] | Precise geocoding [29,31], other disturbance signals [31], cost | Research [14,37,39] | High sensitivity to small displacements [14], non-invasive [14] | Precise geocoding [31,49], other disturbance signals [31], high costs |
| Glaciers | Research [42–46] | Spatial and temporal sampling [42], long range measurements [45] | Phase unwrapping [42,43], unhomogeneus atmosphere effects [43], | Early stage research [12] | Ice height difference, spatial sampling, remote sensing [12] | Low precision (metric order) [12] |
| Snow covered slopes | Early stage research [47–50] | Under certain condition snow water equivalent can be estimated from phase [47,48], avalanche detection [47,35], snow depth [47,49,50], snow avalanche volume [49,50] | Wet snow [47,48, 50], snow water equivalent only with complementary data [48] | Not applicable | | |

2011[29]), there is not a reliable solution for slopes characterized by non-homogeneous atmospheric effects.

Other important GBSAR applications are urban monitoring (Pieraccini et al., 2004[34]; Tapete et al., 2013[35]; Pipia et al., 2013[36]), structure monitoring (Tarchi et al., 1997[14]), dam monitoring (Tarchi et al., 1999[14]; Alba et al., 2008[38]; Luzi et al., 2010c[39]) and dike monitoring (Takahashi et al., 2013[40]; Monserrat, 2012[31]). In addition to the high spatial and temporal sampling capability, a major GBSAR advantage for urban and structural monitoring is the capability to detect, remotely, small displacements. An optimal GBSAR data exploitation in urban and structural monitoring demands a precise geocoding of the measured points. The geocoding quality depends on the quality of the used DEM (Rödelsperger, 2011[29]; Monserrat, 2012[31]). An excellent solution can be provided by terrestrial laser scanners (Tapete et al., 2013[35]; Jungner, 2009[41]). Another solution can be the DEM generated by using GBSAR interferometry (Noferini et al., 2007; Rödelsperger, 2011[29]), even though the achievable quality is much worse than that of laser scanners.

The use of GBSAR for studying glaciers has grown on the last few years. Several papers present the potentialities of this technique for measuring changes on a glacier, e.g., (Luzi et al., 2007[42]; Noferini et al., 2009[43]; Hyangsun and Hoonyol, 2011[44]; Strozzi et al., 2012[12]; Voytenko et al., 2012[45]). GBSAR provides a reliable tool for measuring the relative displacements occurred within the glacier body at long ranges and high resolution (Riesen et al., 2011[46]). However, in some cases, the time lapse during consecutive acquisitions, few minutes in most of the available systems, can be too long with respect to the velocity of some parts of the glaciers (Noferini et al., 2009[43]). Although most of the papers related to glacier applications concern C-GBSAR, D-GBSAR has been used to derive the changes on the ice height computing the differences of DEMs generated from different campaigns (Strozzi et al., 2012[12]).

Finally, although it is not exactly related to deformations, there is a group of applications related to snow covered slopes which are based on the same principle of the GBSAR deformation measurements but which are still on an early research stage. They include the measurement of snow water equivalent (Schaffhauser et al., 2008[49]; Luzi et al., 2009[48]) and avalanche detection (Martínez-Vazquez and Fortuny-Guasch, 2008[50]; Martínez-Vazquez, 2008[51]).

## 7. Conclusions

This paper provides a review of GBSAR interferometry for deformation measurement. In the last decade this technique has gained an increasing interest due to its specific characteristics, which make it complementary to many other existing deformation monitoring techniques. The fundamentals of GBSAR interferometry for deformation measurement have been outlined, discussing the main observation equation of this technique. Deriving deformation estimates from the GBSAR observations (i.e., the interferometric phases) is not always straightforward: the main data processing and analysis stages needed to estimate deformations from GBSAR observations have been described. In the same section the two types of GBSAR acquisition modes (continuous and discontinuous GBSAR) have been described and the different GBSAR processing and analysis methods published in the literature have been reviewed. In a subsequent section the specific technical aspects of GBSAR deformation measurement have been discussed, which include the role of phase noise, the importance of phase

unwrapping, the mono-dimensional characteristics of deformation measurements and the fact that GBSAR provides relative deformation measurements. Based on the above sections, the pros and cons of GBSAR for deformation monitoring have been summarized.

A short review of the GBSAR systems described in the literature has then been provided. In this section, a comprehensive list of references has been provided, including both SAR and non-strictly SAR systems. This is complemented by a table that summarizes the main characteristics, e.g., radar type, radar band, range and azimuth resolutions, operating range, etc., of these systems. Finally, a brief review of the main GBSAR applications has been provided. Six main classes of application have been identified, namely open pit slope stability monitoring, landslides, urban monitoring, structure monitoring, glaciers and snow applications, discussing, for each GBSAR application, its degree of maturity, pros and cons.

## Acknowledgements

This work has been partially funded by the Government of Catalonia, through the SAXA project (2010CTP00048) of the Comunitat de Treball dels Pirineus (www.ctp.org), and by the Spanish Ministry of Science and Innovation, through the XLIDE project (IPT-2011-1287-370000) in the framework of the INNPACTO programme.

## References

Alba, M., Bernardini, G., Giussani, A., Ricci, P.P., Roncoronia, F., Scaioni, M., Valgoic, P., Zhangd, K., 2008. Measurement of dam deformations by terrestrial interferometric techniques. Int. Arch. Photogramm., Remote Sens. Spatial Inf. Sci. 37 (part b1), 133–139.

Barla, G., Antolini, F., Barla, M., Mensi, E., Piovano, G., 2010. Monitoring of the Beauregard landslide (Aosta Valley, Italy) using advanced and conventional techniques. Eng. Geol. 116 (3), 218–235.

Berardino, P., Fornaro, G., Lanari, R., Sansosti, E., 2002. A new algorithm for surface deformation monitoring based on small baseline differential SAR interferograms. IEEE Trans. Geosci. Remote Sens. 40 (11), 2375–2383.

Bernardini, G., Ricci, P., Coppi, F., 2007. A ground based microwave interferometer with imaging capabilities for remote measurements of displacements. In: Proc. GALAHAD Workshop Within the 7th Geomatic Week and the 3rd International Geotelematics Fair (GlobalGeo), Barcelona (Spain), 20–23 February.

Bozzano, F., Cipriani, I., Mazzanti, P., Prestininzi, A., 2011. Displacement patterns of a landslide affected by human activities: insights from ground-based InSAR monitoring. Nat. Hazards 59 (3), 1377–1396.

Brown, S., Quegan, S., Morrison, K., Bennett, J., Cookmartin, G., 2003. High-resolution measurements of scattering in wheat canopies—implications for crop parameter retrieval. IEEE Trans. Geosci. Remote Sens., 1602–1610.

Casagli, N., Farina, P., Leva, D., Nico, G., Tarchi, D., 2003. Ground-based SAR interferometry as a tool for landslide monitoring during emergencies. Proc. IGARSS 4, 2924–2926.

Casagli, N., Catani, F., Del Ventisette, C., Luzi, G., 2010. Monitoring, prediction, and early warning using ground-based radar interferometry. Landslides 7 (3), 291–301.

Corsini, A., Berti, M., Monni, A., Pizziolo, M., Bonacini, F., Cervi, F., Truffelli, G., 2013. Rapid assessment of landslide activity in Emilia Romagna using GB-InSAR short surveys. In: Landslide Science and Practice. Springer, Berlin, pp. 391–399.

Crosetto, M., Crippa, B., Biescas, E., Monserrat, O., Agudo, M., Fernández, P., 2005. Land deformation monitoring using SAR interferometry: state-of-the-art. Photogrammetrie, Fernerkundung und Geoinf. 6, 497–510.

Crosetto, M., Monserrat, O., Cuevas, M., Crippa, B., 2011. Spaceborne differential SAR interferometry: data analysis tools for deformation measurement. Remote Sens. 3, 305–318.

Crosetto, M., Monserrat, O., Luzi, G., Cuevas-Gonzalez, M., Devanthery, N., 2014. A non-interferometric procedure for deformation measurement using GB-SAR imagery. IEEE Geosci. Remote Sens. Lett. 11 (1), 34–38.

Del Ventisette, C., Intrieri, E., Luzi, G., Casagli, N., Fanti, R., Leva, D., 2011. Using ground based radar interferometry during emergency: the case of the A3 motorway (Calabria Region, Italy) threatened by a landslide. Nat. Hazards Earth Syst. Sci. 11, 2483–2495.

Farina, P., Leoni, L., Babboni, F., Coppi, F., Mayer, L., Ricci, P., 2011. IBIS-M, an innovative radar for monitoring slopes in open-pit mines. In: Proc., Slope Stability 2011: International Symposium on Rock Slope Stability in Open Pit Mining and Civil Engineering, Vancouver (Canada), 18–21September.

Farina, P., Leoni, L., Babboni, F., Coppi, F., Mayer, L., Coli, N., Thompson, C., 2012. Monitoring engineered and natural slopes by ground-based radar: methodology, data processing and case studies review. In: Proc. SHIRMS 2012: Southern Hemisphere International Rock Mechanics Symposium, Sun City (South Africa), 15–17 May.

Farina, P., Coli, N., Yön, R., Eken, G., Ketizmen, H., 2013. Efficient real time stability monitoring of mine walls: the çöllolar mine case study. In: Proc. International Mining Congress and Exhibition of Turkey, Antalya (Turkey), 16–19 April, pp. 11–117.

Ferretti, A., Prati, C., Rocca, F., 2001. Permanent scatterers in SAR interferometry. IEEE Trans. Geosci. Remote Sens. 39 (1), 8–20.

Fortuny, J., Sieber, A.J., 1994. Fast algorithm for a near field synthetic aperure radar processor. IEEE Trans. Antennas Propagation 41, 1458–1460.

Fortuny-Guasch, J., 2009. A fast and accurate far-field pseudopolar format radar imaging algorithm. IEEE Trans. Geosci. Remote Sens. 47 (4), 1187–1196.

Ghiglia, D.C., Pritt, M.D., 1998. Two-dimensional phase unwrapping: theory, algorithms, and software. Ed. Wiley, New York (USA).

Hanssen, R., 2001. Radar interferometry. Ed. Kluwer Academic Publishers, Dordrecht (The Netherlands).

Herrera, G., Fernandez-Merodo, J.A., Mulas, J., Pastor, M., Luzi, G., Monserrat, O., 2009. A landslide forecasting model using ground based SAR data: the Portalet case study. Eng. Geol. 105 (3–4), 220–230.

Hyangsun, H., Hoonyol, L., 2011. Motion of Campbell glacier, east Antarctica, observed by satellite and ground-based interferometric synthetic aperture radar. In: 3rd International Asia-Pacific Conference on Synthetic Aperture Radar (APSAR) 1 (4), pp. 26–30.

Iannini, L., Guarnieri, A.M., 2011. Atmospheric phase screen in ground-based radar: statistics and compensation. IEEE Geosci. Remote Sens. Lett. 8 (3), 537–541.

IDS. 2013. IBIS Guardian Software v. 02.00 – User Manual. IDS Ingegneria Dei Sistemi S.p.A., Pisa, Italy.

Iglesias, R., Fabregas, X., Aguasca, A., Mallorqui, J.J., Lopez-Martinez, C., Gili, J.A., Corominas, J., 2013. Atmospheric phase screen compensation in ground-based SAR with a multiple-regression model over mountainous regions. IEEE Trans. Geosci. Remote Sens. 99, 1–14.

Intrieri, E., Di Traglia, F., Del Ventisette, C., Gigli, G., Mugnai, F., Luzi, G., Casagli, N., 2013. Flank instability of Stromboli volcano (Aeolian Islands, Southern Italy): integration of GB-InSAR and geomorphological observations. Geomorphology 201, 60–69.

Jungner, A., 2009. Ground-based synthetic aperture radar data processing for deformation measurement. Master thesis, Royal Institute of Technology (KTH), Division of Geodesy. Stockholm, Sweden.

Lee, H., Lee, J.H., Kim, K.E., Sung, N.H., Cho, S.J., 2013. Development of a truck-mounted arc-scanning synthetic aperture radar. IEEE Trans. Geosci. Remote Sens. (In press).

Leva, D., Nico, G., Tarchi, D., Fortuny, J., Sieber, A.J., 2003. Temporal analysis of a landslide by means of a ground-based SAR interferometer. IEEE Trans. Geosci. Remote Sens. 41, 745–752.

Leva, D., Rivolta, C., Binda Rossetti, I., Kuzuoka, S., Mizuno, T., 2005. Using a ground based interferometric synthetic aperture radar (GBinSAR) sensor to monitor a landslide in Japan. Proc. IGARSS 6, 4096–4099.

Lin, Q., Vesecky, J.F., Zebker, H.A., 1992. New approaches in interferometric SAR data processing. IEEE Trans. Geosci. Remote Sens. 30, 560–567.

Lukin, K., Mogyla, A., Palamarchuk, V., Vyplavin, P., Lukin, S., Kozhan, E., 2009. Monitoring of Kiev St. Sophia cathedral using Ka-band ground based noise SAR. In: Proc. 6th Radar Conference, EURAD2009, Rome, Italy, pp. 215–217.

Luzi, G., Pieraccini, M., Mecatti, D., Noferini, L., Guidi, G., Moia, F., Atzeni, C., 2004. Ground-based radar interferometry for landslides monitoring: atmospheric and instrumental decorrelation sources on experimental data. IEEE Trans. Geosci. Remote Sens. 42 (11), 2454–2466.

Luzi, G., Pieraccini, M., Mecatti, D., Noferini, L., Macaluso, G., Galgaro, A., Atzeni, C., 2006. Advances in ground based microwave interferometry for landslide survey: a case study. Int. J. Remote Sens. 27 (12), 2331–2350.

Luzi, G., Pieraccini, M., Mecatti, D., Noferini, L., Macaluso, G., Tamburini, A., Atzeni, C., 2007. Monitoring of an alpine glacier by means of ground-based SAR interferometry. IEEE Geosci. Remote Sens. Lett. 4 (3), 495–499.

Luzi, G., Noferini, L., Mecatti, D., Macaluso, G., Pieraccini, M., Atzeni, C., Schaffhauser, A., Fromm, R., Nagler, T., 2009. Using a ground-based SAR interferometer and a terrestrial laser scanner to monitor a snow-covered slope: results from an experimental data collection in Tyrol (Austria). IEEE Trans. Geosci. Remote Sens. 47, 382–394.

Luzi, G., Monserrat, O., Crosetto, M., Copons, R., Altimir, J., 2010a. Ground-based SAR interferometry applied to landslide monitoring in mountainous areas. In: Proc. Mountain Risks Conference, Florence, Italy, 24–26 November.

Luzi, C., Del Ventisette, C., Casagli, N., 2010b. Monitoring deformation of the sciara del fuoco (Stromboli) through ground-based radar interferometry. Acta Vulcanologica 22 (1), 77–84.

Luzi, G., Crosetto, M., Monserrat, O., 2010c. Advanced Techniques for Dam Monitoring. In: Proc. II International Congress on Dam Maintenance and Rehabilitation, Zaragoza, Spain, 23–25 November.

Martínez-Vazquez, A., Fortuny-Guasch, J., 2008. A GB-SAR processor for snow avalanche identification. IEEE Trans. Geosci. Remote Sens. 46 (11), 3948–3956.

Martínez-Vazquez, A., 2008. Snow cover monitoring techniques with GB-SAR. PhD thesis, Universitat Politècnica de Catalunya.

Mecatti, D., Macaluso, G., Barucci, A., Noferini, L., Pieraccini, M., Atzeni, C., 2010. Monitoring open-pit quarries by interferometric radar for safety purposes. In: Proc. European Radar Conference (EuRAD), Paris, France, 30 September–1 October, pp. 37–40.

Meta A., Trampuz C., 2009. Metasensing compact, high resolution interferometric SAR sensor for commercial and scientific applications. In: Proc. of the 7th Radar Conference, EURAD, Rome, Italy, pp. 21–24.

Monserrat, O., 2012. Deformation measurement and monitoring with ground-based SAR. PhD thesis, Technical University of Catalonia.
Monserrat, O., Moya, J., Luzi, G., Crosetto, M., Gili, J.A., Corominas, J., 2013. Non-interferometric GB-SAR measurement: application to the Vallcebre landslide (eastern Pyrenees, Spain). Nat. Hazards Earth Syst. Sci. 13 (7), 1873–1887.
Nico, G., Leva, D., Antonello, G., Tarchi, D., 2004. Ground-based SAR interferometry for terrain mapping: theory and sensitivity analysis. IEEE Trans. Geosci. Remote Sens. 42 (6), 1344–1350.
Nico, G., Leva, D., Fortuny-Guasch, J., Antonello, G., Tarchi, D., 2005. Generation of digital terrain models with a ground-based SAR system. IEEE Trans. Geosci. Remote Sens. 43 (1), 45–49.
Noferini, L., 2004. Processing techniques of microwave data acquired by continuous wave stepped frequency radar. PhD thesis, Università degli Studi di Firenze.
Noferini, L., Pieraccini, M., Mecatti, D., Macaluso, G., Atzeni, C., 2005a. Long term and slide monitoring by ground based SAR interferometer. Int. J. Remote Sens. 27, 1893–1905.
Noferini, L., Pieraccini, M., Mecatti, D., Luzi, G., Tamburini, A., Broccolato, M., Atzeni, C., 2005b. Permanent scatters analysis for atmospheric correction in ground-based SAR interferometry. IEEE Trans. Geosci. Remote Sens. 43 (7), 1459–1471.
Noferini, L., Pieraccini, M., Mecatti, D., Macaluso, G., Luzi, G., Atzeni, C., 2007. DEM by ground-based SAR interferometry. IEEE Geosci. Remote Sens. Lett. 4 (4), 659–663.
Noferini, L., Takayama, T., Mecatti, D., Macaluso, G., Luzi, G., Atzeni, C., 2008. Analysis of ground-based SAR data with diverse temporal baselines. IEEE Trans. Geosci. Remote Sens. 46 (6), 1614–1623.
Noferini, L., Mecatti, D., Macaluso, G., Pieraccini, M., Atzeni, C., 2009. Monitoring of belvedere glacier using a wide angle GB-SAR interferometer. J. Appl. Geophys. 68 (2), 289–293.
Noon, D., Harries, N., 2007. Slope stability radar for managing rock fall risks in open cut mines. In: Proc. Large Open Pit Mining Conference Perth, Australia, 10–11 September 2007.
Ozdemir, C., Yigit, E., Demirci, S., 2011. A comparison of focusing algorithms for ground based SAR. In: Proc PIERS. Marrakesh, Morocco, 20–23 March, pp. 548–553.
Pieraccini, M., Luzi, G., Atzeni, C., 2001. Terrain mapping by ground-based interferometric radar. IEEE Trans. Geosci. Remote Sens. 39 (10), 2176–2181.
Pieraccini, M., Luzi, G., Mecatti, D., Fratini, M., Noferini, L., Carissimi, L., Franchioni, G., Atzeni, C., 2004. Remote sensing of building structural displacements using a microwave interferometer with imaging capability. Non Destruct. Test. Eval. 37 (7), 545–550.
Pieraccini, M., 2013. Real beam vs. synthetic aperture radar for slope monitoring. In: Proc. PIERS 2013, Stockholm, Sweden, 12–15 August.
Pipia, L., Fabregas, X., Aguasca, A., Lopez-Martinez, C., 2013. Polarimetric temporal analysis of urban environments with a ground-based SAR. IEEE Trans. Geosci. Remote Sens. 51 (4), 2343–2360.
Reale, D., Serafino, F., Pascazio, V., 2009. An accurate strategy for 3-D ground-based SAR imaging. IEEE Geosci. Remote Sens. Lett. 6 (4), 681–685.
Riesen, P., Strozzi, T., Bauder, A., Wiesmann, A., Funk, M., 2011. Short-term surface ice motion variations measured with a ground-based portable real aperture radar interferometer. J. Glaciol. 57 (201), 53–60.
Rödelsperger, S., Becker, M., Gerstenecker, C., Läufer, G., Schilling, K., Steineck, D., 2010. Digital elevation model with the ground-based SAR IBIS-L as basis for volcanic deformation monitoring. J. Geodyn. 49 (3–4), 241–246.
Rödelsperger, S., 2011. Real-time processing of ground based synthetic aperture radar (GB-SAR) measurements. PhD thesis, Technische Universität Darmstadt.
Schaffhauser, A., Adams, M., Fromm, R., Jörg, P., Luzi, G., Noferini, L., Sailer, R., 2008. Remote sensing based retrieval of snow cover properties. Cold Reg. Sci. Technol. 54 (3), 164–175.
Schulz, W.H., Coe, J.A., Shurtleff, B.L., Panosky, J., Farina, P., Ricci, P.P., Barsacchi, G., 2012. Kinematics of the Slumgullion landslide revealed by ground-based InSAR surveys. In: Proc. Landslides and Engineered Slopes: Protecting Society through Improved Understanding – the 11th International and 2nd North American Symposium on Landslides and Engineered Slopes, Banff (Canada), 3–8 June, pp. 1273–1279.
Severin, J., Eberhardt, E., Leoni, L., Fortin, S., 2011. Use of ground-based synthetic aperture radar to investigate complex 3-D pit slope kinematics. In: Proc. Slope Stability 2011: International Symposium on Rock Slope Stability in Open Pit Mining and Civil Engineering, Vancouver, Canada, 18–21 September.
Strozzi, T., Werner, C., Wiesmann, A., Wegmuller, U., 2012. Topography mapping with a portable real-aperture radar interferometer. IEEE Geosci. Remote Sens. Lett. 9 (2), 277–281.
Takahashi, K., Matsumoto, M., Sato, M., 2013. Continuous observation of natural-disaster-affected areas using ground-based SAR interferometry. IEEE J. Sel. Top. Appl. Earth Observations Remote Sens. 6 (3), 1286–1294.
Tapete, D., Casagli, N., Luzi, G., Fanti, R., Gigli, G., Leva, D., 2013. Integrating radar and laser-based remote sensing techniques for monitoring structural deformation of archaeological monuments. J. Archaeol. Sci. 40 (1), 176–189.
Tarchi, D., Ohlmer, E., Sieber, A.J., 1997. Monitoring of structural changes by radar interferometry. J. Res. Nondestruct. Eval. 9 (4), 213–225.
Tarchi, D., Rudolf, H., Luzi, G., Chiarantini, L., Coppo, P., Sieber, A.J., 1999. SAR interferometry for structural changes detection: a demonstration test on a dam. In: Proc. IGARSS 1999, Hamburg, Germany, pp. 1522–1524.
Tarchi, D., Casagli, N., Fanti, R., Leva, D., Luzi, G., Pasuto, A., Pieraccini, M., Silvano, S., 2003a. Landslide monitoring by using ground-based SAR interferometry: an example of application. Eng. Geol. 68 (1–2), 15–30.
Tarchi, D., Casagli, N., Moretti, S., Leva, D., Sieber, A.J., 2003b. Monitoring landslide displacements by using ground-based radar interferometry: application to the Ruinon landslide in the Italian alps. J. Geophys. Res. 108 (10), 1–14.
Tarchi, D., Antonello, G., Casagli, N., Farina, P., Fortuny-Guasch, J., Guerri, L., Leva, D., 2005. On the use of ground-based SAR interferometry for slope failure early warning: the Cortenova rock slide (Italy). In: In Landslides: Risk Analysis and Sustainable Disaster Management. Ed. Springer, Berlin Heidelberg, pp. 337–342.
Tarchi, D., Lukin, K., Fortuny-Guash, J., Mogyla, A., Vyplavin, P., Sieber, A., 2010. SAR imaging with noise. IEEE Trans. Aerosp. Electron. Syst. 46 (3), 1214–1225.
Tarchi, D., Olivieri, F., Sammartino, P.F., 2013. MIMO radar and ground-based SAR imaging systems: equivalent approaches for remote sensing. IEEE Trans. Geosci. Remote Sens. Lett. 51 (1).
Ulaby, F.T., Moore, R.K., Fung, A.K., 1986. Microwave Remote Sensing: Active and Passive. In: Volume Scattering and Emission Theory, Advanced Systems and Applications. Artech House Inc, Dedham, Massachusetts, vol. III.
Voytenko, D., Dixon, T.H., Werner, C., Gourmelen, N., Howat, I.M., Tinder, P.C., Hooper, A., 2012. Monitoring a glacier in southeastern Iceland with the portable terrestrial radar interferometer. Proc. IGARSS, 3230–3232.
Zhou, Z.S., Boerner, W.M., Sato, M., 2004. Development of a ground-based polarimetric broadband SAR system for noninvasive ground-truth validation in vegetation monitoring. IEEE Trans. Geosci. Remote Sens. 42 (11), 1803–1810.